



Synthesis of new benzimidazolium salts with tunable emission intensities and their application as fluorescent probes for Fe³⁺ in pure aqueous media



Amita Krishan Lal, Marilyn Daisy Milton*

Department of Chemistry, University of Delhi, Delhi 110007, India

ARTICLE INFO

Article history:

Received 22 November 2013

Revised 25 January 2014

Accepted 27 January 2014

Available online 5 February 2014

Dedicated to Professor Sakae Uemura on his 73rd birthday

Keywords:

Photoinduced electron transfer (PET)

Benzimidazolium

Fluorescence

Fe³⁺ sensors in water

ABSTRACT

A series of novel, water-soluble benzimidazolium salts with common 'fluorophore-spacer-receptor' PET design has been synthesized. Despite the common PET scaffold these benzimidazolium salts displayed diverse emission intensities in pure aqueous solutions. The observed emission intensities were found to be influenced by the functionalized alkyl side arms present on the benzimidazolium ring. These benzimidazolium salts were also found to act as selective sensors for Fe³⁺ ions over other metal ions like Na⁺, K⁺, Ca²⁺, Mg²⁺, Ba²⁺, Al³⁺, Cr³⁺, Co²⁺, Ni²⁺, Mn²⁺, Zn²⁺, Pb²⁺, Ag⁺, Cu²⁺ and Hg²⁺ in pure aqueous media.

© 2014 Elsevier Ltd. All rights reserved.

Photoinduced electron transfer (PET) is a long-range electron transfer from the receptor to the fluorophore in the excited state.^{1–3} The PET design includes a 'fluorophore-spacer-receptor' architecture, where the electron donor (receptor) and an electron acceptor (fluorophore) are linked together by a flexible spacer. In the excited state, electron transfer from the electron donor to the electron acceptor may quench the fluorescence from the fluorophore. The efficiency of the PET process strongly depends upon a number of factors such as conformational changes, polarity modulation, hydrogen bonding, distance between the fluorophore and the receptor.⁴

During the past few years, the fluorescent chemosensors with PET design have been used in metal ion detection due to their high selectivity, sensitivity and precision.^{5,6} Amongst the various transition metals, iron is one of the most important elements for the environment and living systems due to its significant role in various metabolic and electron transfer processes of the cells.^{7,8} Thus, considerable efforts have been made towards the development of iron sensing probes. A variety of fluorescent iron sensing probes based on coumarin,⁹ thiacalixarene,¹⁰ anthracene,¹¹ fluoranthene,¹² rhodamine,¹³ 1,8-naphthalimide,¹⁴ etc. have been developed. However, the poor water solubility of these fluorescent

probes limits their application under physiological conditions. Till date, very few Fe³⁺ sensors in pure aqueous media have been reported.^{15–18} Therefore, the development of sensors which can work in pure aqueous media is a challenging task, and hence, needs attention.

As part of our research work on the synthesis and applications of benzimidazolium salts, we have designed a series novel, water-soluble benzimidazolium salts with a common 'fluorophore-spacer-receptor' PET scaffold. The ligand design incorporates the benzimidazolium fluorophore unit attached to a pyridine receptor arm through a methylene spacer. Pyridine can act as a receptor by transferring lone pair of electrons on nitrogen to the benzimidazolium ring by PET mechanism. With an aim to fine-tune the PET process, we have introduced functionalized alkyl chains as side arms on the PET scaffold by N-quaternization of the benzimidazole ring (Fig. 1). Herein, we report the synthesis of new water-soluble benzimidazolium salts with tunable fluorescence intensities and their use as selective sensors for Fe³⁺ in pure aqueous media.

Highly water-soluble benzimidazolium salts **2–6** were synthesized in moderate to good yields by heating 2-(1*H*-benzimidazol-1-ylmethyl)pyridine (**1**)¹⁹ with the corresponding alkyl halides in a suitable solvent for 24–48 h (Scheme 1).

The structures of **2–4** were confirmed by X-ray crystallographic analysis.²⁰ The molecular structures of **2–4** are shown in Figure S1.

* Corresponding author. Tel.: +91 11 27667794 140.

E-mail address: mdmilton@chemistry.du.ac.in (M.D. Milton).

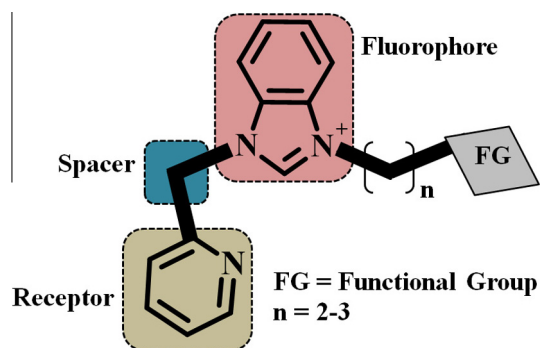
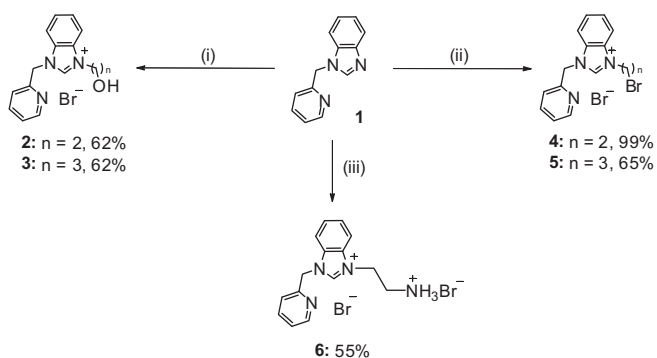


Figure 1. Design of benzimidazolium based NHC ligands with common PET scaffold.



Scheme 1. Reagents and conditions: (i) 2-bromoethanol/3-bromopropanol, acetonitrile, reflux, 48 h; (ii) 1,2-dibromoethane/1,3-dibromopropane, reflux, 24–48 h; (iii) 2-bromoethylamine hydrobromide, acetonitrile, reflux, 48 h.

The pyridine side arm, attached to the benzimidazolium ring through a methylene spacer, was common in **2–4**. Whereas, the other side arm had hydroxyethyl, hydroxypropyl and bromoethyl groups in **2**, **3** and **4** respectively. In all the structures, both the pyridine and the functionalized alkyl side arms were positioned on the same side of the benzimidazolium ring. The pyridine ring in **2**, **3** and **4** was inclined at an angle of 89.5°, 89.0° and 66.8°, respectively to the benzimidazolium ring.

A symmetrical sheet-like packing was observed for these benzimidazolium salts where the bromide ions were sandwiched between the layers of the benzimidazolium units (Fig. 2). The key parameters of **2–4** are summarized in Table S1; the bond parameters were found to be similar to those reported in other

benzimidazolium salts^{21–23} (Tables S2 and S3). However, the small variation amongst these ligands was due to the difference in the packing effects. A strong (C–H)⁺⋯Br[−] ionic hydrogen bonding (2.93 Å) was observed between carbenic hydrogen and bromide ion in **2** whereas, no such interactions were observed in **3** and **4**. Rather, the hydrogen bonding was observed between the hydroxyl group and bromide ion in ligand **3** (Table S4). Also, many intermolecular C–H⋯Br contacts were observed for these ligands (**2–4**). Moreover, in **2**, the two benzimidazolium units present in the unit cell dimerized together due to the antiparallel arrangement of the benzimidazolium rings (Fig. S2). This also led to π ⋯ π and C–H⋯ π interactions in the solid state (Fig. S3). However, in **3**, despite the offset arrangement of benzimidazolium rings, no π ⋯ π and C–H⋯ π interactions could be observed, due to improper orientation of the benzimidazolium rings (Fig. S4). Similarly, in the crystal packing of **4**, two benzimidazolium units dimerized together due to the C–H⋯ π interactions but no π ⋯ π interactions were seen (Fig. S2).

The UV absorption maxima for **2–6** (5.0×10^{-5} mol dm^{−3}) in water were observed at 262 nm with shoulder peaks at 257, 268 and 280 nm (Fig. S5). Despite the common PET scaffold, **2–6** showed diverse emission intensities ranging from low to very high fluorescence intensities in 100% aqueous solutions with the emission maxima around 373–375 nm with high values of Stokes shift (Fig. 3 and Table S5). The emission intensities decreased in the order **2** > **3** > **5** > **6** > **4**.

Although, fluorescence studies were carried out in solution phase, we reasoned that the single crystal X-ray diffraction studies may provide an insight into the relative position of the fluorophore and the receptor in these molecules (**2–4**). The crystal structures revealed that the pyridine rings were inclined at an angle of 89.5°, 89.0° and 66.8° to the benzimidazolium rings in **2**, **3** and **4**, respectively (Fig. 4). This conformational difference in the angle of inclination may play a role in the fluorescence emission of these ligands. In case of **2** and **3**, pyridine rings were inclined nearly perpendicular (89.5° and 89.0°, respectively) to the plane of the benzimidazolium ring. Thus, the π -orbitals of the benzimidazolium ring and lone pair of electrons on pyridine nitrogen were spatially disposed in the same plane. This reduced the rate of intersystem crossing and hence, their effectiveness as electron transfer source for the PET process.²⁴ Thus, higher emission intensities were observed with **2** and **3**. However, in case of ligand **4**, the angle of inclination was 66.8° hence the possibility of partial PET process increased. The heavy atom effect of bromine may also contribute to the quenching of fluorescence in **4**. The difference in the angle of inclination between pyridine and benzimidazolium rings in **2–4** can be attributed to the influence of the functionalized alkyl

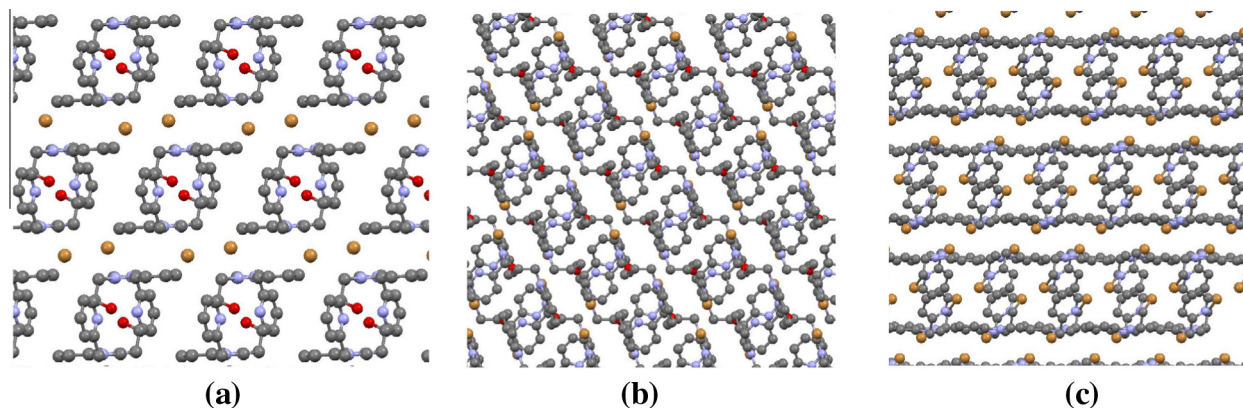


Figure 2. Symmetrical sheet-like packing of: (a) compound **2** when viewed along crystallographic axis *c*; (b) compound **3** when viewed along crystallographic axis *b* and (c) compound **4** when viewed along crystallographic axis *b*.

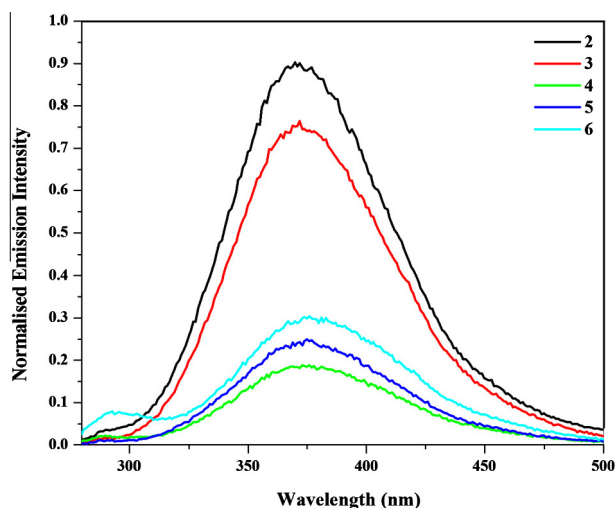


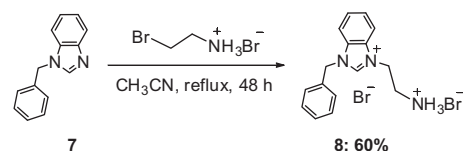
Figure 3. Normalized fluorescence spectra of **2–6** and **8** ($5.0 \times 10^{-5} \text{ mol dm}^{-3}$) in water with excitation and emission slit width of 5 nm.

side arm on the orientation of the pyridine ring w.r.t. the benzimidazolium ring.

In order to understand the role of the pyridine ring as receptor in sensing mechanism, we synthesized **8**, where the pyridine ring was replaced by a benzene ring. Ligand (**8**) was synthesized in 60% yield by refluxing 1-benzylbenzimidazole (**7**)²⁵ with 2-bromoethylamine hydrobromide in acetonitrile solvent for 48 h (Scheme 2).

The UV absorption maxima for **8** ($5.0 \times 10^{-5} \text{ mol dm}^{-3}$) in water were observed at 272 nm with a shoulder peak at 280 nm (Fig. S5). The emission maxima in water were observed at 374 nm. A comparison of the emission intensities of **6** and **8** revealed that **8** showed much higher emission intensity as compared to **6** (Fig. 5), in fact, **8** showed the highest emission intensity amongst all the ligands (**1–8**). This could be attributed to the absence of receptor (pyridine ring) in **8**, which removed the possibility of any PET process through the receptor as compared to **6** which had a pyridine ring as receptor. However, in both **6** and **8**, the ammonium group present in the alkyl side chain might undergo PET process up to some extent upon partial conversion to the amino group on hydrolysis in aqueous solution.²⁶

Next, we studied the interaction of various metal ions with the benzimidazolium salts **2–6** and **8** in aqueous media. All the synthesized benzimidazolium salts **2–6** and **8** were capable of sensing Fe^{3+} . However, detailed studies were carried out with **3** and **8** by the addition of various metal ion solutions to the aqueous solution



Scheme 2. Synthetic route for **8**.

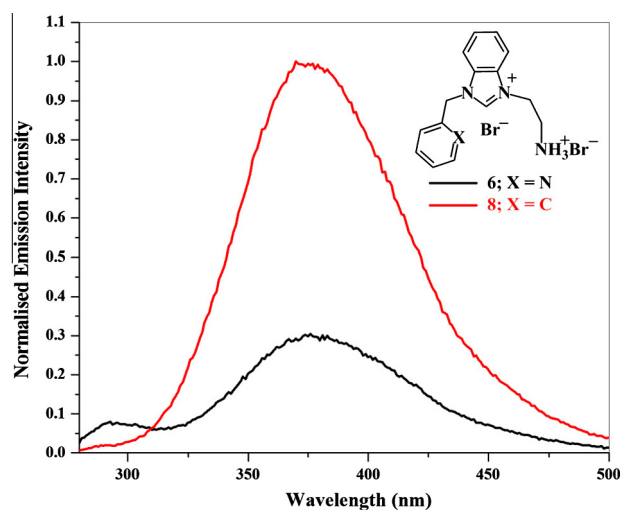


Figure 5. A comparison of emission spectra of **6** and **8** ($5.0 \times 10^{-5} \text{ mol dm}^{-3}$) in water with excitation and emission slit width of 5 nm.

of the benzimidazolium salts. It was observed that addition of 33 equiv of Na^+ , K^+ , Ca^{2+} , Mg^{2+} , Ba^{2+} , Cr^{3+} , Mn^{2+} , Ni^{2+} , Zn^{2+} , Cu^{2+} , Hg^{2+} , Co^{2+} , Ag^+ , Al^{3+} and Pb^{2+} did not produce any major changes in the emission spectra of **3** and **8**. But the addition of 33 equiv of Fe^{3+} quenched the emission intensity significantly (Figs. 6 and S6). Thus, these benzimidazolium salts can act as fluorescent probes for Fe^{3+} by 'turn-off' mechanism. Quenching was observed due to the paramagnetic nature of Fe^{3+} , which increased the rate of the nonradiative pathways through energy transfer or electron transfer when present in close vicinity of the probe.²⁷ The quenching efficiency of Fe^{3+} was unaffected by the counter ion (Cl^- and NO_3^-). The complexation studies with Fe^{3+} were carried out with its nitrate salt. It is noteworthy that a substantial quenching was also observed with Fe^{2+} .

Further, the selectivity of the probes for Fe^{3+} was studied by the addition of a solution of Fe^{3+} ions to the solution of probes **3** or **8** with other metal ions such as Na^+ , K^+ , Ca^{2+} , Mg^{2+} , Ba^{2+} , Al^{3+} , Cr^{3+} ,

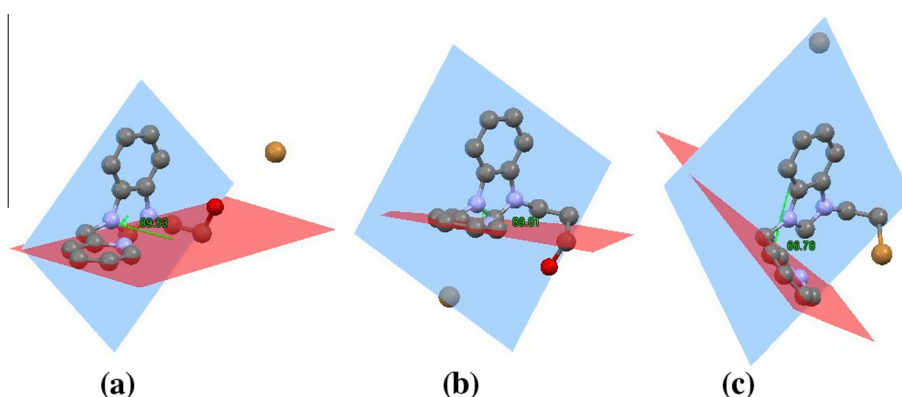


Figure 4. Molecular structure diagrams of (a) **2**, (b) **3** and (c) **4** showing the angle of inclination between pyridine and benzimidazolium rings.

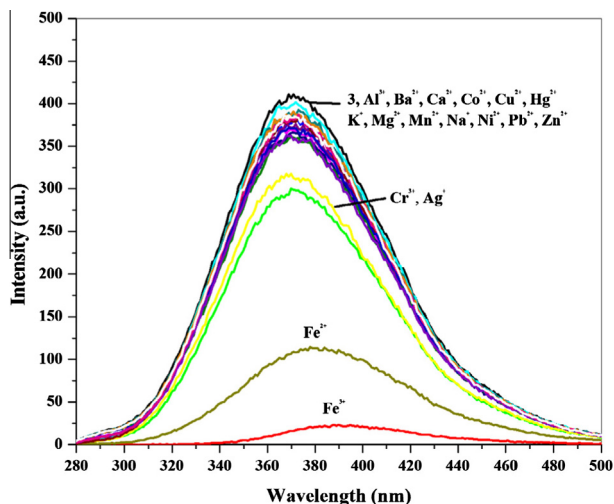


Figure 6. Fluorescence spectra of **3** (1.0×10^{-4} mol dm $^{-3}$) on addition of 33 equiv of different metal ions in water.

Fe^{2+} , Co^{2+} , Ni^{2+} , Mn^{2+} , Zn^{2+} , Pb^{2+} , Ag^+ , Cu^{2+} and Hg^{2+} . It was found that the quenching efficiency of Fe^{3+} remained unaffected in the presence of these ions including the competitive metal ions like Cu^{2+} , Cr^{3+} , Co^{2+} and Fe^{2+} (Figs. 7 and S7). Thus, it was concluded that both probes **3** and **8** were highly selective for Fe^{3+} ions in pure aqueous media.

To determine the affinity of probes and the quantitative sensitivity range, fluorescence titration experiments were performed for Fe^{3+} . During the fluorescence titration, the progressive addition of Fe^{3+} diminished the emission intensity gradually (Fig. S8). Further the detection limit^{28–30} was calculated from the titration data by plotting a graph between $((I_{\text{max}} - I)/(I_{\text{max}} - I_{\text{min}}))$ and $\log[\text{Fe}^{3+}]$. A linear regression curve in the range of 8.3 μM –1.6 mM afforded an intercept of -5.02 and -4.74 at the ordinate axis, which corresponds to the detection limit of 9.45×10^{-6} M and 1.80×10^{-5} M

for **3** and **8**, respectively (Fig. S9). These data indicate that probe **3** has high sensitivity for Fe^{3+} detection as compared to **8**.

The 1:1 stoichiometry of metal and ligand in probes **3** and **8** was confirmed by Job's plot (Fig. S10). Probe **3** can possibly interact with Fe^{3+} through the hydroxyl group, carbenic carbon and pyridine nitrogen. While probe **8** may interact with Fe^{3+} through the carbenic carbon³¹ and the amino group (formed due to hydrolysis of ammonium group in water). The availability of one additional binding site in **3** suggests a stronger binding to Fe^{3+} as compared to **8**, which was further confirmed by the calculation of binding constant using Benesi–Hildebrand equation.³² A good linear relationship ($R^2 = 0.9983$ and 0.9994) was obtained from the graphs plotted between $I_0/I_0 - 1$ and $1/[\text{Fe}^{3+}]$ for **3** and **8** and the binding constants were calculated to be 3.12 and 2.14×10^3 M $^{-1}$ for **3** and **8**, respectively (Fig. S11).

In conclusion, a series of novel highly water-soluble benzimidazolium salts with a common 'fluorophore-spacer-receptor' PET design was synthesized with an aim to fine-tune the PET process in these ligands. By varying the functionalized alkyl side arm attached to the PET scaffold, we were successful in modulating the emission intensities of these benzimidazolium salts in aqueous solutions. Also, these benzimidazolium salts demonstrated high selectivity for Fe^{3+} over 15 other metal ions in pure aqueous media.

Acknowledgments

We gratefully acknowledge financial support from the University of Delhi, India and the Department of Science and Technology, India. A.K.L. also acknowledges the Council for Scientific and Industrial Research, India for Junior and Senior Research Fellowships. The authors are grateful to USIC-CIF, University of Delhi for NMR spectral data and single crystal XRD data.

Supplementary data

Supplementary data (^1H , ^{13}C NMR spectroscopic and HRMS data) associated with this article can be found, in the online version, at <http://dx.doi.org/10.1016/j.tetlet.2014.01.127>.

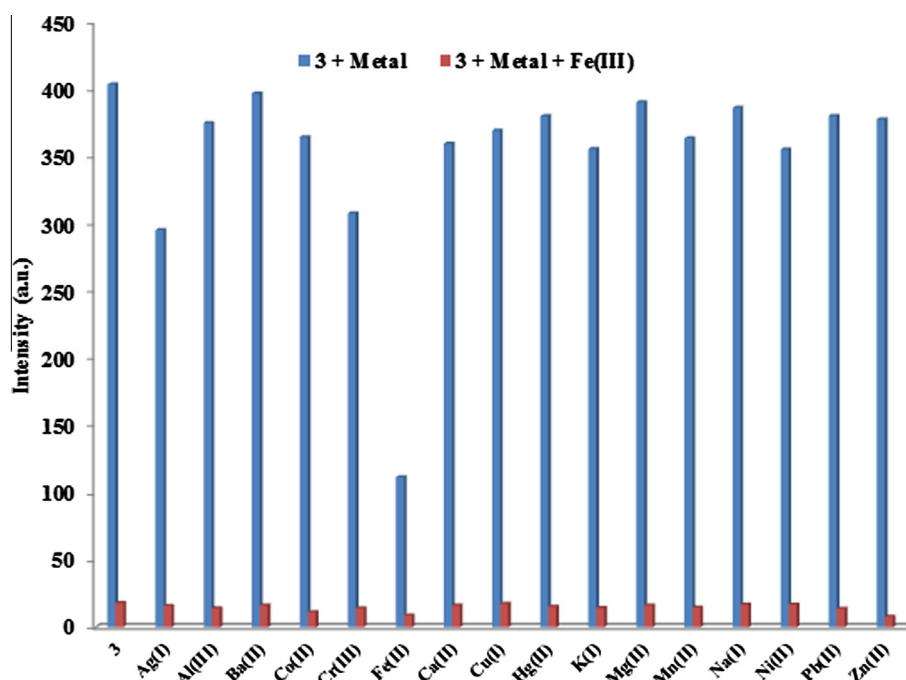


Figure 7. Selectivity of **3** for Fe^{3+} on addition of different metal ions.

References and notes

1. de Silva, A. P.; Gunaratne, H. Q. N.; Gunlaugsson, T.; Huxley, A. J. M.; McCoy, C. P.; Rademacher, J. T.; Rice, T. E. *Chem. Rev.* **1997**, *97*, 1515.
2. de Silva, A. P.; Vance, T. P.; West, M. E. S.; Wright, G. D. *Org. Biomol. Chem.* **2008**, *6*, 2468.
3. de Silva, A. P.; Moody, T. S.; Wright, G. D. *Analyst* **2009**, *134*, 2385.
4. Bissell, R. A.; de Silva, A. P.; Gunaratne, H. Q. N.; Lynch, P. L. M.; Maguire, G. E. M.; Sandanayake, K. R. A. S. *Chem. Soc. Rev.* **1992**, *21*, 187.
5. Amendola, V.; Fabbrizzi, L.; Foti, F.; Licchelli, M.; Mangano, C.; Pallavicini, P.; Poggi, A.; Sacchi, D.; Taglietti, A. *Coord. Chem. Rev.* **2006**, *250*, 273.
6. Valeur, B.; Leray, I. *Coord. Chem. Rev.* **2000**, *205*, 3.
7. Crichton, R. R. *Inorganic Biochemistry of Iron Metabolism* In Horwood, E., Ed.; John Wiley & Sons: New York, 1991.
8. Sahoo, S. K.; Sharma, D.; Bera, R. K.; Crisponi, G.; Callan, J. F. *Chem. Soc. Rev.* **2012**, *41*, 7195.
9. Lim, N. C.; Pavlova, S. V.; Bruckner, C. *Inorg. Chem.* **2009**, *48*, 1173.
10. Kumar, M.; Kumar, R.; Bhalla, V.; Sharma, P. R.; Kaur, T.; Qurishi, Y. *Dalton Trans.* **2012**, *41*, 408.
11. Lee, D. Y.; Singh, N.; Jang, D. O. *Tetrahedron Lett.* **2011**, *52*, 1368.
12. Li, Z.; Zhang, L.; Li, X.; Guo, Y.; Ni, Z.; Chen, J.; Wei, L.; Yu, M. *Dyes Pigm.* **2012**, *94*, 60.
13. Yang, Z.; She, M.; Yin, B.; Cui, J.; Zhang, Y.; Sun, W.; Li, J.; Shi, Z. *J. Org. Chem.* **2012**, *77*, 1143.
14. Yang, L.; Yang, W.; Xu, D.; Zhang, Z.; Liu, A. *Dyes Pigm.* **2013**, *97*, 168.
15. Danjou, P. E.; Lyskawa, J.; Delattre, F.; Becuwe, M.; Woisel, P.; Ruellan, S.; Fourmentin, S.; Cazier-Dennin, F. *Sens. Actuators, B* **2012**, *171–172*, 1022.
16. Mao, J.; Wang, L.; Dou, W.; Tang, X.; Yan, Y.; Liu, W. *Org. Lett.* **2007**, *22*, 4567.
17. Qin, C.; Cheng, Y.; Wang, L.; Jing, X.; Wang, F. *Macromolecules* **2008**, *41*, 7798.
18. Mao, J.; He, Q.; Liu, W. *Talanta* **2010**, *80*, 2093.
19. Jarusiewicz, J.; Yoo, K. S.; Jung, K. W. *Synlett* **2009**, 482.
20. *Crystal data for 2*: C₁₅H₁₆BrN₃O, M = 334.22, triclinic, a = 8.8102(8), b = 9.6686(10), c = 10.2553(10) Å, α = 82.241(8), β = 70.803(9), γ = 62.905(10)°, V = 732.19(12) Å³, T = 298(2) K, space group P-1, Z = 2, 6195 reflections measured, 2581 unique reflections (R_{int} = 0.0278). Final R₁ = 0.0391 (I > 2σ(I)), wR(F²) = 0.0799. CCDC 961641.
Crystal data for 3: C₁₆H₁₈BrN₃O, M = 348.24, monoclinic, a = 9.1199(5), b = 17.9089(8), c = 10.2501(5) Å, β = 106.985(6)°, V = 1601.10(14) Å³, T = 298(2) K, space group P2₁/n, Z = 4, 12,181 reflections measured, 3257 independent reflections (R_{int} = 0.0290). Final R₁ = 0.0385 (I > 2σ(I)), wR(F²) = 0.0769. CCDC 961640.
Crystal data for 4: C₁₅H₁₅Br₂N₃, M = 397.12, monoclinic, a = 10.5193(8), b = 14.8862(9), c = 11.4646(10) Å, β = 114.682(10)°. V = 1631.3(2) Å³, T = 298(2) K, space group P2₁/c, Z = 4, 7664 reflections measured, 3195 unique reflections (R_{int} = 0.0293). Final R₁ = 0.0571 (I > 2σ(I)), wR(F²) = 0.1663. CCDC 885195.
21. Jahnke, M. C.; Pape, T.; Hahn, F. E. *Eur. J. Inorg. Chem.* **2009**, *20*, 1960.
22. Lee, K. M.; Lee, C. K.; Lin, I. J. B. *Cryst. Eng. Commun.* **2010**, *12*, 4347.
23. Bai, Y.; Zhang, B. G.; Duan, C. Y.; Dang, D. B.; Meng, Q. *New J. Chem.* **2006**, *30*, 266.
24. Yoshino, J.; Kano, N.; Kawashima, T. *J. Org. Chem.* **2009**, *74*, 7496.
25. Kore, R.; Srivastava, R. *J. Mol. Catal. A: Chem.* **2011**, *345*, 117.
26. He, X.; Zhu, B. Y.; Huang, J.; Zhao, G. X. *J. Colloid Interface Sci.* **1999**, *220*, 338.
27. Li, L.; She, N.; Fei, Z.; So, P.; Wang, Y.; Cao, L.; Wu, A.; Yao, Z. *J. Fluoresc.* **2011**, *21*, 1103.
28. Shortreed, M.; Kopelman, R.; Kuhn, M.; Hoyland, B. *Anal. Chem.* **1996**, *68*, 1414.
29. Lin, W.; Yuan, L.; Long, L.; Guo, C.; Feng, J. *Adv. Funct. Mater.* **2008**, *18*, 2366.
30. Caballero, A.; Martinez, R.; Lloveras, V.; Ratera, I.; Vidal-Gancedo, J.; Wurst, K.; Tarraga, A.; Molina, P.; Veciana, J. *J. Am. Chem. Soc.* **2005**, *127*, 15666.
31. Zhang, H.; Xie, L.; Yan, W.; He, C.; Cao, X.; Duan, C. *New J. Chem.* **2009**, *33*, 1478.
32. Benesi, H. A.; Hildebrand, J. H. *J. Am. Chem. Soc.* **1949**, *71*, 270.